UNIVERSITY OF TARTU

Faculty of Physics and Chemistry

Institute of Experimental Physics and Technology

ALEKSANDR LISSOVSKI

Spectroscopic diagnostics of pulsed discharge in high–pressure rare gas mixtures

Master of Science thesis

Optics and Spectroscopy

Supervisor: Alexey Treshchalov,
Ph. D., Head of laboratory,
Institute of Physics, University of Tartu

TARTU 2004

CONTENTS

1. INTRODUCTION

Many efforts have been pursued for the research and development of rare gas excimer VUV lasers. The laser emission originates from diatomic molecules (Ar_2 –126 nm, Kr_2 – 148 nm, Xe_2 – 172 nm) that are bound in the excited electronic state but have repulsive potentials in the ground states. Unfortunately operation of such rare gas excimer lasers has been achieved so far only by unpractical electron-beam pumping. The main difficulties in operating of such lasers are due to the following: 1. The stimulated emission cross sections are smaller than those of well-known rare gas halide excimers by about an order of magnitude, 2. Formation channel of excimers is limited to a three-body reaction: $R^* + R + R \rightarrow R_2^* + R$. Therefore, a high-power density (~20 MW/cm^3) must be deposited by the discharge into a high-pressure gas (~10 bar) for VUV laser operation.

Ignition of homogeneous high-current discharge in high-pressure gas mixtures is a serious physical and technical problem. Several criteria should be satisfied to avoid constrictions in the discharge (intense and uniform preionization, short rise time for the discharge voltage and current, uniform electric field in the discharge gap). Many of these applied problems are very difficult to solve without the detailed understanding of basic physical and chemical processes that determine the properties and evolution of discharge plasma. Therefore the reliable spectroscopic diagnostic data for the non-stationary, non-equilibrium discharge plasma is of great importance for successful development of rare gas excimer VUV light sources.

Continuum emission of rare gases in UV-VIS spectral range is well known but the origin and interpretation of this so-called third continuum is still the subject of discussions. Most experimental third continuum spectra were obtained using a hard ionizer - electron or heavy ion beam. This excitation is characterized by production of excited rare gas ions R^{+*} as primary excited species through collisions of neutral atoms with energetic beam particles and secondary electrons. All other subsequent plasma chemical processes are connected with downstream energy flow kinetics. In this case the dominant contribution to the third continuum emission comes from transitions of excited rare gas molecular ions R_2^{+*}.

Discharge is essentially different from beam excitation. Due to exponential dependence of electron collision excitation (ionization) rates, lower atomic states have usually much higher population than high-lying atomic and ionic states. In this case main ionization in

plasma is caused by secondary stepwise ionization processes (upstream energy flow: $R^* + e \rightarrow R^+ + e$) and density of excited rare gas ions R^{+*} is rather small. Therefore, the nature of continuum emission in discharge and beam-excited rare gases could be different.

Specific aims of this work are: 1. Experimental diagnostics of electron density in high-pressure (up to 10 bar) rare gas highly ionized plasma, determination of their influence to the VUV emission of rare gas excimers; 2. Studying of spectral-time behavior of UV-VIS continuum emission in high-current discharges for different rare gas mixtures and revealing of the origin of continuum.

2. THEORETICAL SURVEY

2.1. Types of plasma emission spectra

Photons of light appear and disappear at radiative transitions of electrons between different energy states. Let's consider the system consisting of an electron and “atomic rest” or a positive ion. Schematic diagram of electron energy states is shown in Fig. 1. Arrows show several possible types of radiative transitions: 1) bound-bound, 2) bound-free, 3) free-free.

Bound-bound transitions of electron between discrete atomic levels lead to the origin of different spectral lines in spontaneous emission and absorption. Bound-free transitions represent photoionization and photorecombination processes:

$$A + h\nu \leftrightarrow A^+ + e$$
$$A^* + h\nu \leftrightarrow A^+ + e \qquad (1)$$

where A, A* atoms in the ground and excited states correspondently. Free-free transitions represent bremsstrahlung radiation and inverse bremsstrahlung absorption of photons by electrons during coulomb ion-electron interaction. Free-free transitions take place also between electrons interacted with neutral atoms in scattering processes. In weakly ionized plasma with a high atom density ions play a negligible role for bremsstrahlung processes. Free-free and bound-free transitions give continuous spectra, because either initial, or final, or both electronic states lay in continuum [1].

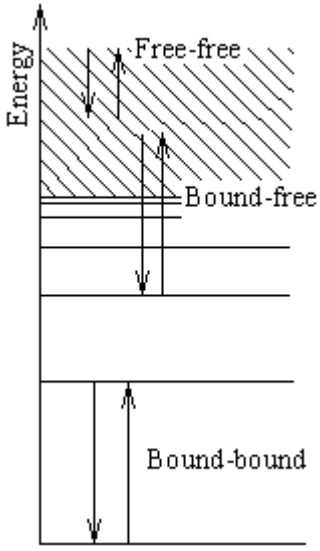

Fig. 1. Levels and transitions scheme of electrons in the atom

Let's consider the main types of radiations, which can be observed in emission spectrum of low temperature weakly ionized plasma of rare gases.

2.2. Photorecombination continuum

At capture of electrons with velocities in the interval v to v + dv to the n atomic level a photon with energy hν radiates and corresponding radiation energy $J(\nu)_n$ from 1 cm^3 in 1 s is [1]

$$J(\nu)_n = C\, h\nu\, N_i\, N_e\, \sigma_{pn}\, F(\nu)\, \nu d\nu \qquad (2)$$

$$h\nu = |E_n| + m\nu^2/2 \qquad (3)$$

where E_n – energy difference between n atomic level and ionization threshold, N_i – density of positive atomic ions, N_e – electron density, σ_{pn} – electron photorecombination cross section, F(ν) – electron velocity Maxwellian distribution, m – electron mass, C – constant.

Photon of energy hν can be radiated during electron capture to different atomic levels, if electron kinetic energy is in accordance with condition (3). For the calculation of photorecombination radiation in the spectral interval $\nu \div \nu + d\nu$ the expression (2) should be summed by all levels. For example, a photon of energy $h\nu > |E_1|$ can be radiated by capture to any level. The photon of lower energy, $h\nu < |E_1|$ is radiated only by capture to higher levels $n \geq n^*$. The lowest of them n^* is determined by condition $|E_{n^*}| \leq h\nu < |E_{n^*-1}|$. Also, following various captures the energy $J_{rec}d\nu$ radiates from 1 cm^3 in 1 s in the spectral interval dν.

$$J_{rec}(\nu)d\nu = d\nu \sum_{n^*(\nu)}^{\infty} J(\nu)_n \qquad (4)$$

The spectrum of recombination continuum is shown in Fig. 2. During the scanning of the frequency from some value $\nu_n = |E_n|/h$, the number of items in sum is firstly constant and intensity of radiation follows the electron Maxwellian distribution function according to formula (1). As soon as ν reaches the value ν_{n-1}, which correspond the capture of electron to n-1 level, one more item is added to the sum and function $J_{rec}(\nu)$ makes a jump. After the last jump at $\nu = \nu_1$ the emission decreases monotonously.

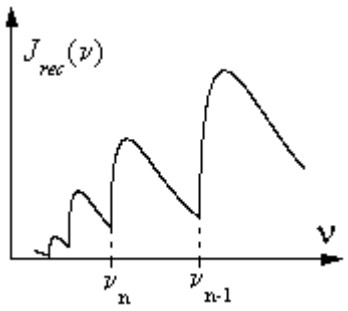

Fig. 2. Spectrum of photorecombination emission

The photorecombination mechanism is not effective because of rather small cross sections (about 10^{-21} cm^2). In laboratory plasma conditions it plays seldom significant role as a main recombination mechanism.

2.3. Bremsstrahlung from electron-atom collisions

For electron energy comparable to or lower than atomic excitation energies, bremsstrahlung emission strongly depends on the details of the electron-atom interaction and full theoretical description is very complicated.

The emission of electromagnetic radiation in weakly ionized plasma is due mainly to collisions of electrons with atoms. Typically, this is so in plasmas with ionization degree of the order of or smaller than 0.1 per cent (at electron temperature of about 1 eV). The emission is originated from the acceleration of an electron in the force field of the target particle. In the limit of low-energy photons and using the phase-shift approximation, the neutral bremstrahlung cross section $Q_B(\nu,E)$ is expressed as [2]

$$Q_B(\nu, E) = \frac{8 r_e}{3c} \frac{E}{h\nu} \left(1 - \frac{h\nu}{E}\right)^{1/2} \left[q_0(E - h\nu) + \left(1 - \frac{h\nu}{E}\right) q_0(E) \right] \tag{5}$$

where r_e is the classical electron radius, c is the speed of light and q_0 is the electron elastic scattering cross section as a function of electron energy.

The formula for the spectral emission coefficient for neutral bremsstrahlung is [2]

$$\eta(\nu) = N_a N_e h\nu \int_{h\nu}^{\infty} E^{1/2} \, Q_B(\nu, E) \, F(E) \, dE \tag{6}$$

where $\eta(\nu)$ is the energy radiated per unit time from unit volume in the spectral interval of $d\nu$, F(E) – electron energy distribution function.

Only few experiments under the discharge excitation have been made for measurement of bremsstrahlung continuum spectra over a wide range of wavelengths [2, 3, 4]. The intensity of bremsstrahlung emission is proportional to densities of electrons and neutral particles. Spectrum of bremsstrahlung emission contains also valuable information about the temperature of electrons, which is often difficult to measure by other plasma diagnostics methods.

2.4. Dissociative recombination

The process of dissociavite recombination may be represented schematically by the reaction

$$AB^+ + e \Leftrightarrow AB'' \rightarrow A + B \tag{7}$$

In a collision of an electron with a molecular ion AB^+ (see Fig. 3) a temporary state of the neutral molecule AB″ is formed. This state is unstable, since an electron can be reemitted through autoionization. However it is extremely likely that the state AB″ will dissociate through a repulsive potential curve into neutral atoms rather than reionize by emitting of electron. As a result electron can be trapped and two neutral atoms can be formed, often in excited states.

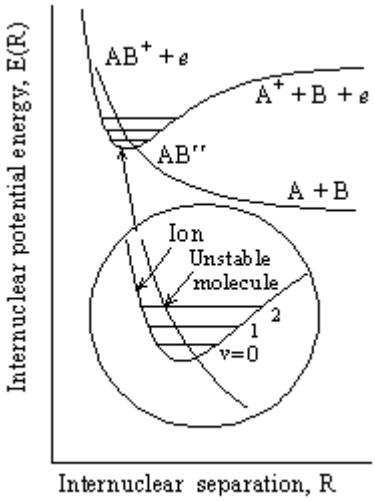

Fig. 3. Schematic of the potential energy curves involved in the dissociative recombination process.

For electron recombination with atomic ions at moderate densities there is no stabilization mechanism of comparable efficiency, and for this reason the recombination rate for molecular ions is normally several orders of magnitude greater than that for atomic ions [1, 5]. Process of dissociative recombination plays a determining role in the mechanism of excitation of the rare-gas excimer lasers, working on electronic transitions between the excited and ground, repulsive terms of excimer molecules.

2.5. Stark effect

Broadening and shift of most atomic and ionic lines occur in electrical discharge plasma. The charged particles (electrons and ions) on distance of about collision radius generate large local electric fields, which are the reason of the Stark effect [6]. Measuring of Stark profiles allows one to determine electron density for different types of plasma. Electron density is found by comparing measured and calculated widths of several tabulated lines. In the case of linear Stark effect electrons and ions make comparable contributions to the line broadening. Formula for the electron density is the following [6]:

$$N_e = C(N_e, T_e) \cdot \Delta\lambda_S^{3/2} \qquad (8)$$

where $\Delta\lambda_S$ – Stark broadening width (FWHM), $C(N_e,T_e)$ – coefficient that depends weakly on electron density and temperature.

In the case of quadratic Stark effect the ionic part of broadening is usually small and not taken into account. Electron density in this case is expressed by the simplified formula:

$$N_e = C(N_e, T_e) \cdot \Delta\lambda_S \qquad (9)$$

Inaccuracy of Stark broadening method for electron density measurement is in the range of 20 – 30 %. In the case of hydrogen H_β line (486.8 nm) inaccuracy is rather small (about 7 %), for H_α line (656.3 nm) inaccuracy is about 15 % because for these lines more exact calculations were carried out [6].

3. EXPERIMENTAL ARRANGEMENT AND METHODS

3.1. Pumping circuit and gas handling system

Since the discharge in high-pressure inert gases tends to constrict due to ionization and thermal instabilities, specially designed fast discharge circuits should be used to avoid the constriction and to achieve high-efficient VUV emission. The discharge electrical driving circuit, shown in Fig. 4, is a thyratron-switched charge-transfer scheme with storage C_0 and peaking C_P capacitors [7]. The circuit permits to achieve a steep (~ 40 ns) voltage growth (~$3 \cdot 10^{11}$ V/s) at relatively low charging voltage (up to 20 kV). VUV automatic preionization is performed by a sliding discharge on Al_2O_3 (sapphire) plate that is placed laterally of the cathode electrode. The volume discharge is produced between the two parallel nickel cylindrically profiled electrodes. The length of electrodes is 24 cm with a gap spacing of 0.14 cm. Pulse repetition rate of our discharge device (up to 50 Hz) is limited mainly by the high voltage power supply, no special gas circulation is necessary. The discharge chamber (volume of ~5 l), made of aluminium, and relevant gas handling system were evacuated by turbomolecular pumping system to 10^{-5} mbar. He, Kr, Ar gases with 99.998 % purity were used in our experiments. In all our experiments the gas temperature was at ~300 K.

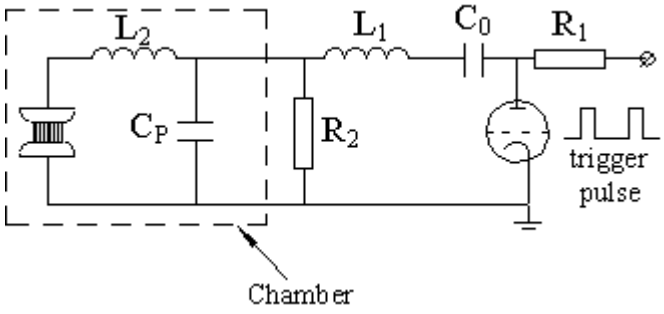

R_1 =1 MΩ R_2 = 200 Ω

C_0 = 4.3 nF C_P = 7.7 nF

L_1 = 160 nH L_2 = 2.36 nH

Maximal stored energy

$$\frac{C_0 U_{max}^2}{2} \approx 860 \text{ mJ}$$

Fig. 4. Electrical driving circuit

Present electrical scheme for pulsed pumping is the most optimal one of several earlier probed circuits. In ideal charge-transfer regime the charge from the storage capacitor is transferred to the peaking capacitor just before the breakdown of the gap and all the pumping energy $C_p U_{br}^2/2$ is stored in the peaking capacitor. The regime of the energy loading to the discharge plasma depends on values L_2, C_p and plasma resistance R_{pl}. In electrotechnically matched conditions, when the plasma resistance is equal to double circuit impedance $R_c = 2\rho = 2(L_2/Cp)^{1/2} \approx 1.1$ Ohm, the minimal time of energy loading is achieved (see Fig. 5). This time is about $\pi \cdot (L_2 C_p)^{1/2} \approx 12$ ns. If $R_{pl} > R_c$, then long-

term pumping without oscillations will take place. If $R_{pl} < R_c$, then long-term pumping with several oscillations will take place. In this mismatched regime the polarity of the pumping voltage between electrodes changes twice during the period $2\pi(L_2C_p)^{1/2}$. Fig. 5 shows all 3 regimes of energy loading.

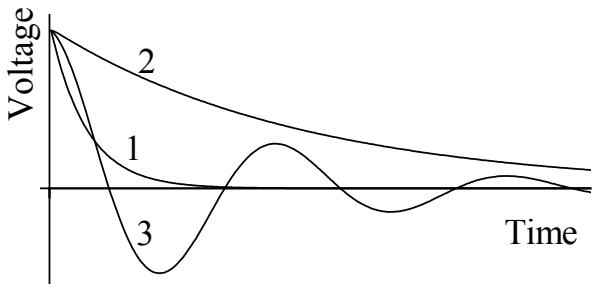

1. $R_{pl} \approx R_c$, matched pumping
2. $R_{pl} > R_c$, long-term pumping without oscillations
3. $R_{pl} < R_c$, long-term non-matched pumping with oscillations

Fig. 5. Different energy loading regimes from the peaking capacitor to the plasma

3.2. Apparatus

A schematic of the experimental setup is shown in Fig. 6. UV-VIS spontaneous emission from the volume discharge plasma is detected through the MgF_2 window by the compact 0.3 m, f/4 Shamrock 303i spectrograph (Andor Technology) with 300 l/mm grating, resolution 0.27 nm/pixel; 1200 l/mm grating, resolution 0.06 nm/pixel; 2400 l/mm holographic grating, resolution 0.02 nm/pixel and gated ICCD camera Intraspec V (Andor Technology). Spectral fragment for the broad continuum, selected by the spectrograph, is restricted to about 170 nm by the size of ICCD photocathode 18 mm and spectrograph dispersion for 300 l/mm grating. Maximal spectral resolution of the system is about 0.06 nm (with 2400 l/mm grating). The available UV-VIS spectral range, determined by the ICCD photocathode is 200-850 nm. This range is possible to cover with four partly overlapped spectra using 300 l/mm grating. The minimal gate width of the ICCD camera is 2.2 ns.

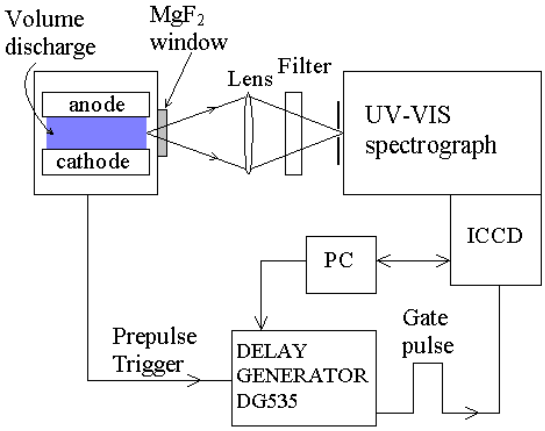

Fig. 6. A schematic diagram of the experimental UV-VIS apparatus.

Discharge and ICCD gate pulses are synchronized by a computer controlled delay generator DG-535 (Stanford Research Systems Inc.) with a total jitter of about ± 1 ns.

VUV spectra were measured by VUV 0.5 m, f/12 M12 monochromator with a concave 1200 l/mm grating (spectral resolution of 0.03 nm) and solar-blind photomultiplier tube R 1080 (Hamamatsu) (time resolution of 3 ns). 400 MHz Tektronix 380 digitizer connected with a computer, measured kinetics of spontaneous emission.

3.3. Calibration of the UV-VIS system

As we want to measure spectral distribution of the broad continuum, spectral sensitivity of the UV-VIS system is necessary to be carefully performed. The tungsten filament (TRS 2860) and deuterium (DDS-30) lamps are used for calibration. Intensity distribution in emission spectra of these lamps is tabulated. Tungsten lamp can be considered as a source with a homogeneous surface radiance. DDS lamp is a source of light with the discharge size of about 2x2x3 mm^3 and inhomogeneous volume radiance. We find that emission spectra of the DDS lamp from the middle point and periphery zones of the discharge are strongly different. Usually the tabulated data for deuterium lamps are given for the emission spectrum from the middle point of the discharge. This point is very difficult to focus into the entrance slit of the monochromator without inputs from the periphery zones. An other problem of calibration by DDS lamp is a strong chromatic aberration of the quarts condenser lens. Even small changes of the lens focus position influence strongly the shape of emission spectra in the UV range. Due to these problems VUV system was not spectrally calibrated.

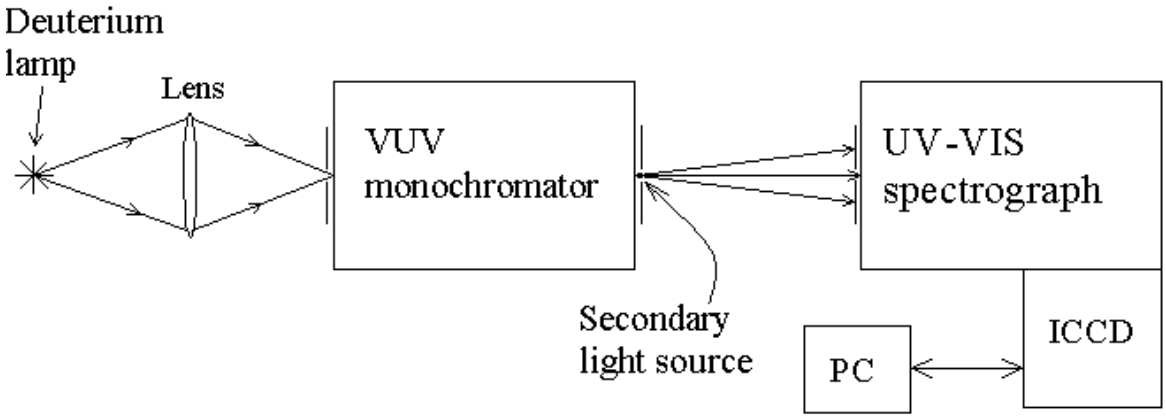

Fig. 7. Set-up for the spectral calibration of the UV-VIS apparatus

Careful calibration was performed for UV-VIS system by the following procedure. Firstly, the calibration in the UV spectral range (200–350 nm) was organized by replacing the volume discharge source in Fig. 6 with a system as shown in Fig. 7, consisted of the deuterium DDS lamp and VUV monochromator with 0.2 mm entrance slit. The output slit of 0.2 mm serves as a secondary light source (without focusing lens) for UV-VIS spectrograph. The spectral intensity distribution of this source was measured by yellow lumogen S0790 powder, which emission has a constant quantum yield for UV excitation photons. Secondly, tungsten filament lamp was used for calibration in 300–850 nm spectral range without focusing lens to avoid the problem with chromatic aberration. Emission of tungsten lamp is considered as black body radiation at temperature 2860 K. Finally, both apparatus functions were compared, normalized and connected in the range of overlapping 280–320 nm. The final spectral sensitivity calibration curve of UV-VIS system (Shamrock with 300 l/mm grating + ICCD) is plotted on Fig. 8.

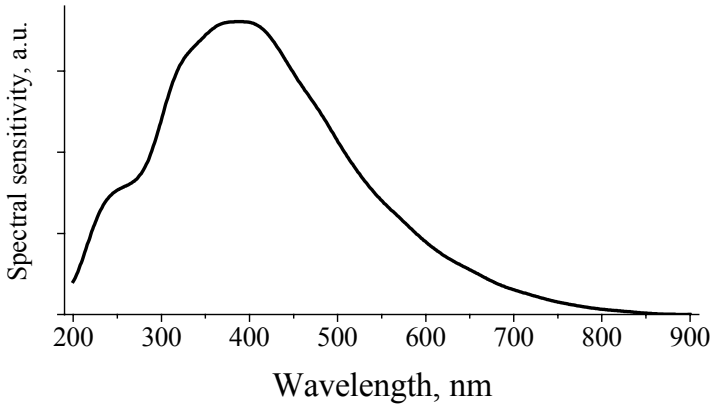

Fig. 8. Spectral sensitivity curve for UV-VIS system

4. RESULTS AND DISCUSSION

4.1. Time behavior of UV-VIS continuum emission and electron density in F_2 - containing gas mixtures

Spectra of continuous emission for the volume discharge of rare gases and their mixtures at pressure 1–8 bar were measured in the range 200–850 nm with UV-VIS spectrograph. These data were corrected on the spectral sensitivity of the registration system (see curve in Fig. 8).

Let's consider firstly fluorine-containing mixtures, characterized by a high rate of electron disappearance.

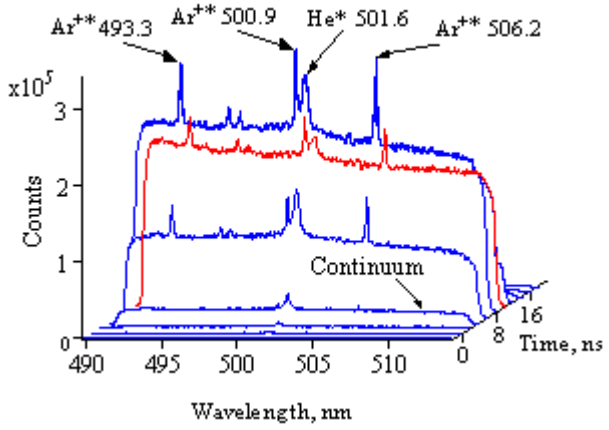

Fig. 9a Time-resolved emission spectra of the discharge of ArF laser gas mixture (one step 2 ns, gate 2.2 ns) [7, 8]

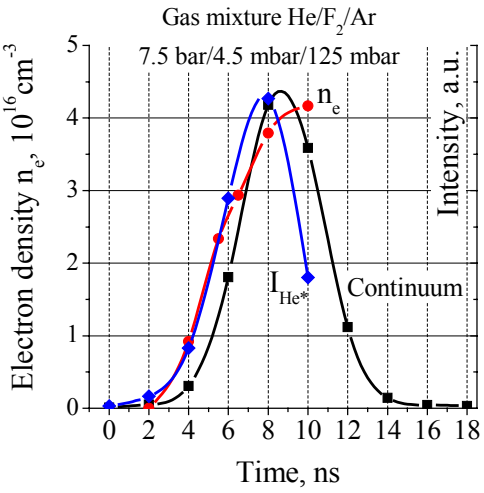

Fig. 9b. Time evolutions of He* emission line 501.6 nm, continuum and calculated density of electrons for the discharge of ArF laser gas mixture

Fig. 9a presents a fragment of time-resolved emission spectra from the volume discharge plasma of ArF laser gas mixture [9]. Zero time corresponds to the beginning of the breakdown. Stark-broadened He^* and narrow Ar^{+*} lines together with strong broad continuum appear during a short discharge excitation pulse - no any long tails exist on the pumping pulse. In contrast to He^* and Ar^* so-called primary components, excited by single-step processes, Ar^{+*} ions (as typical secondary components) appear in the discharge after obvious delay of about 2 ns, when densities of Ar^* atoms and electrons become so high that stepwise excitation-ionization processes successfully compete with direct excitation of Ar from the ground state. From this time the voltage

on the discharge starts to decrease along with an increase of the discharge current and the pumping power maximum is achieved at about 8 ns.

Electron density in the discharge was estimated from Stark broadened profiles of several helium spontaneous emission lines. According to Fig. 9 at the very beginning of the discharge helium line 501.6 nm is mainly pressure broadened and has Lorentzian shape with FWHM of about 0.25 nm. At higher electron density Stark broadening adds to the pressure broadening – line becomes broader (up to about 0.6 nm) but the shape remains Lorentzian. Experimental line profiles are fitted by Lorentzian profiles and Stark broadening widths $\Delta\lambda$s (FWHM) are extracted [6]. Electron density is calculated from the formula (9).

Fig. 9b shows time behaviors of emission intensity for helium line 501.6 nm, continuum and density of electrons for the volume discharge of ArF laser. There is a delay of about 2 ns between intensity of helium line 501.6 nm and continuum emission (the same delay as between Ar^* and Ar^{+*} lines). After the maximum of the pumping pulse ($t > 10$ ns) electron temperature decreases and excitation of helium is terminated in the discharge. Measurements for discharges in KrF, F_2 lasers give rather similar time evolution for electron density with maximum of $7 \cdot 10^{16}$ and $6 \cdot 10^{16}$ cm^{-3} [7]. We estimate the accuracy of these data as 20 %. The main source of possible error is a poor signal-to-noise ratio for measured line profiles due to very strong continuum emission and overlapping of helium lines with emission lines from other excited species.

Fig. 10 shows the time evolution of the fragment of spontaneous emission spectra for volume discharges in three different He-based gas mixtures. Several well-known He_2^* molecular bands, He^* lines as well as a strong broad continuum are observed [10]. Continuum is very similar in three different gas mixtures. It is detected mainly during the short pumping pulse. The first peak of emission from low-lying He_2^* states practically coincides with the excitation pulse. We suggest that at high pressure this first peak is caused by direct electron impact excitation of free collision He-He pairs to excited vibronic levels of low-lying He_2^* states. As concerning He_2^* bands, emitted from high-lying molecular states, there are only weak emissions of these bands during the excitation pulse. However, both low-and high-lying He_2^* states are populated effectively in pure He during the recombination downstream flow.

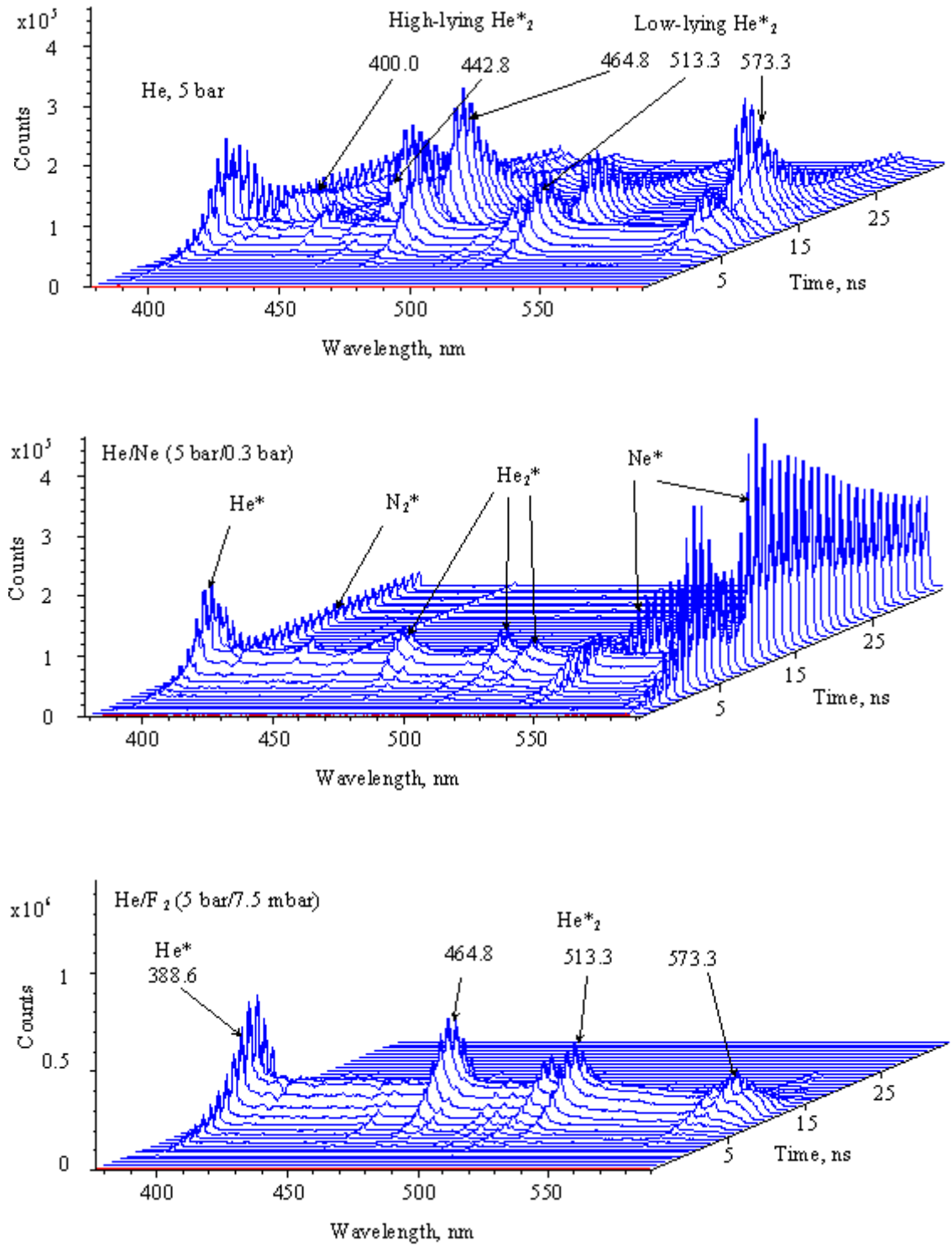

Fig. 10. Time evolution (one step 1 ns, gate 2.2 ns) of emission spectral fragments for volume discharges in different He gas mixtures.

When 0.3 bar of Ne is added to 5 bar He, He_2^* bands strongly decrease on the pumping and recombination stages of the discharge (most of the excitation- recombination flow comes through Ne^* states) but continuum remains nearly the same. This fact is difficult to explain if take into account the assignment of the third continuum as transitions between excited rare gas molecular ions R_2^{+*} (He_2^{+*} ions in our case) [11]. So in helium-based gas mixtures UV-VIS continua are not connected with He_2^{+*} states.

In He discharge with F_2 additives strong He_2^* bands exist only during the excitation pulse and is totally absent in the recombination stage. Main recombination in this electronegative gas mixture goes through the ion-ion recombination channel ($F^+ + F^- + He \rightarrow F_2^* + He$) – key reaction for inversion creation in the F_2 VUV laser. In this case electrons disappear very rapidly due to dissociative attachment reaction

$$F_2 + e^- \rightarrow F^- + F \qquad (10)$$

The rate constant of this reaction is $5 \cdot 10^{-9}$ cm^3 s^{-1} for electron energy of about 1 eV [12]. It means that at 5 mbar of fluorine partial pressure the effective time of electron attachment is about 2 ns.

All these experimental data show that a broad UV-VIS continuum is caused by free electrons.

4.2. Time behavior of VUV–UV emission spectra of the discharge in argon and krypton

VUV emission spectra of excimer molecules Ar_2^* and Kr_2^* at pressures 1–8 bar were measured in the spectral range of 120–300 nm using VUV monochromator and a solar-blind photomultiplier. The maximal pressure, where homogeneous volume discharge was achieved, is about 10 bar for Ar and Kr. At higher pressure volume discharge transforms to bright-white arc discharge. Emission intensity of Ar_2^* and Kr_2^* molecules in the arc discharge is very small, but intensity of UV-VIS continuum is high. It seems that in this highly ionized thermalized plasma, where the gas temperature is comparable with the electron temperature, excimer molecules are strongly vibronically excited and even thermally dissociated in a hot gas.

Fig. 11 shows time-integrated VUV spectra of spontaneous emission of the discharge of Ar and Kr at 1 bar. Spectra are not corrected to VUV system spectral sensitivity. Ar_2^* and Kr_2^* excimers (I and II continua) give the main input to VUV signal in rare gas

discharge plasma. Intensity of the so-called third continuum is rather small comparing with excimer spontaneous emission. Weak narrow lines from traces of gas impurities (C, N, O, H, CO) are also detected in spectra.

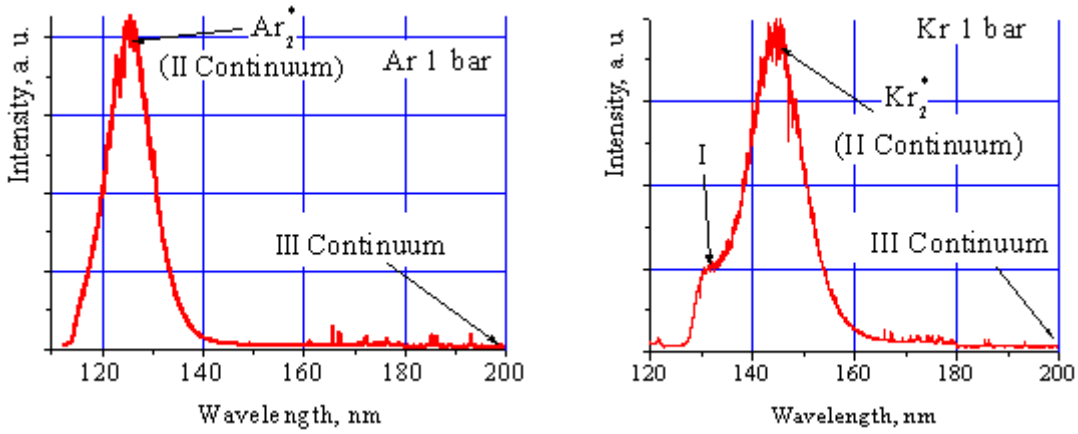

Fig. 11. Time-integrated VUV spectra of spontaneous emission of the discharge in Ar and Kr.

From the viewpoint of using rare-gas discharge plasma as VUV laser active medium, the ideal conditions for lasing effect achievement will be as follows. After a short powerful discharge pumping pulse fast plasma chemical reactions have to create high peak population of vibronically relaxed excimer molecules. It is well known that rates of these reactions increase with the growth of gas density, so spontaneous emission of rare gas excimers has to be shorter and higher intensity [13]. Kinetics of Ar_2^* emission and third continuum, measured at different Ar pressure, are presented in Fig. 12 and 13. These two figures show clearly the following:

1) Intensity of the third argon continuum (258 nm) increases with the pumping power and gas pressure. If we define the ideal (electrotechnically-matched, short and powerful) pumping as a single pulse with a fast recombination tail, then we see that the real pumping is far from ideal. Discharge plasma resistance reduces during the pumping to the magnitude lower than double impedance of the pumping circuit ($\rho \sim 0.6$ Ohm), so a long-term mismatched pumping regime with several ringings is obtained. The frequency of ringing is equal to the oscillation frequency in the pumping contour: $(4\pi^2 L_2 C_p)^{-1/2}$. The best matching is achieved for 8 bar argon discharge.

2) The peak intensity of Ar_2^* excimer emission (126 nm) increases with gas pressure due to the temporal compression of kinetics. Oscillations of spontaneous Ar_2^* emission intensity are in an opposite phase with oscillations of 258 nm continuum (see Fig. 18). The amplitude of these oscillations is the highest for argon discharge at 8 bar in spite of the best electrotechnical matching for 8 bar discharge. This fact we explain as follows: at low pressure (1–2 bar) the plasma chemical reaction rate [14, 15] for Ar_2^* creation (which becomes higher with the growth of the pressure) is slower than the pumping modulation rate (which is fixed by electrotechnical parameters of the pumping circuit). These rates become comparable at higher Ar pressure (4–8 bar).

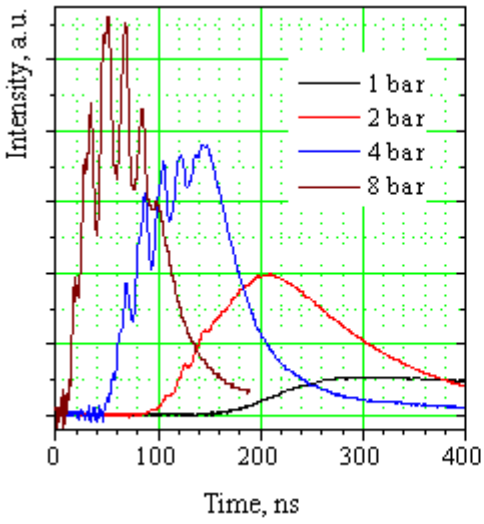

Fig. 12. Time evolution of Ar_2^* (λ=126 nm) spontaneous emission at different Ar pressure

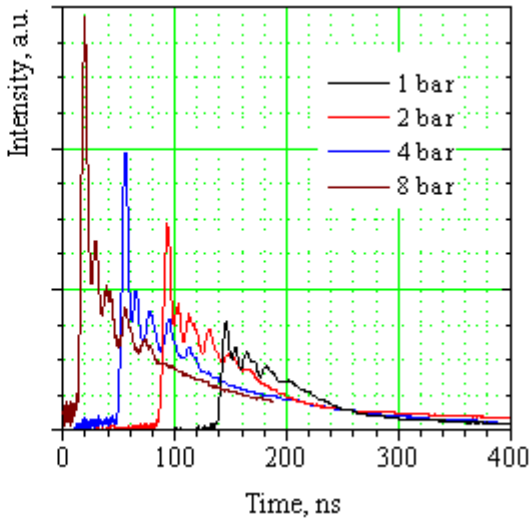

Fig. 13. Time evolution of UV-VIS continuum (λ=258 nm) emission at different Ar pressure

4.3. Electron density estimation from the energy deposition in high-pressure argon discharge

Rough estimation for the electron density in argon plasma can be done from parameters of the pumping circuit (Fig. 4) and measured breakdown voltage U_{br}. Let's assume, that the pumping is matched and all the energy from the peaking capacitor transfers to the volume discharge in the single pumping pulse. If we consider only direct processes of electron multiplication:

$$Ar + e\,(15.76\ \text{eV}) \rightarrow Ar^+ + 2e \qquad (11)$$

then electron density N_e can be estimated from the equation of energy conservation

$$\frac{C_P U_{br}^2}{2} = 15.76\,\text{eV} \cdot N_e V \tag{12}$$

where 15.76 eV is the minimum ionization energy for argon, V is the discharge volume.

In real discharge conditions at high gas pressure the contribution of direct ionization processes (11) is very small. The main mechanism of electron multiplication is usually a stepwise ionization process

$$\begin{aligned} \text{Ar} + e\ (11.55\ \text{eV}) &\rightarrow \text{Ar}^* + e \\ \text{Ar}^* + e\ (4.21\ \text{eV}) &\rightarrow \text{Ar}^+ + 2e \end{aligned} \tag{13}$$

where 11.55 eV is the excitation energy of the lowest metastable state of argon. An electron spends energy firstly for an atom excitation and then for ionization of excited atom. If add up two equations of (13) then result is equal to (11). It means that the minimum energy of 15.76 eV is necessary for a birth of one electron in both processes shown by formula (11) and (13). Taking into account additional energy losses to elastic electron scattering and to the excitation of atomic states the value for birth of one electron-ion pair becomes greater (for example [16] for e-beam pumping the value of about 26 eV is used for Ar). So our rough estimation gives only the upper limit of the maximal electron density. Table 1 shows experimentally measured breakdown voltages, estimated maximal electron densities for various pressures of argon and maximal electron densities measured by Stark broadening of H_α line.

Table 1. Maximal electron density in argon discharge

Pressure, bar	Breakdown voltage, kV	Electron density, 10^{17} cm^{-3}	
		by formula (12)	by Stark broadening
1	2.5	0.28	0.4
2	4	0.73	1.6
4	6	1.6	3–4
6	8	2.9	

Surprisingly, rather good qualitative agreement is observed. The possible disagreement of measured electron density gets higher than estimated one could be explained by:

1. During the breakdown not all the charge is transferred to the peaking capacitor and some additional energy continues to load to the plasma from the storage capacitor.

2. Pumping energy deposition is assumed to be homogeneous, but the real discharge cross-section is even visually inhomogeneous (central part of the discharge is pumped more strongly than peripheral zones).

4.4. Time evolution of UV-VIS continuous emission in argon

Fig. 14 presents the time behavior of a broad UV-VIS continuum emission in argon discharge plasma at 4 bar. These spectra were corrected on the spectral sensitivity that is presented in Fig. 8. The dimension of intensity is proportional to $W \cdot cm^{-3}$ as the most of the literature data about continuous emission are given in these units. The first spectrum with a small signal at t = 0 ns corresponds to the beginning of the breakdown. On the breakdown front signal rises exponentially and at t = 12 ns achieves maximum. There are obvious changes of continuum spectral shape during the discharge: one can compare for example spectrum at t = 40 ns (designated by red color) and next one at t = 44 ns. These changes are explained by the variation of electron temperature in the discharge (for more details, see next paragraph).

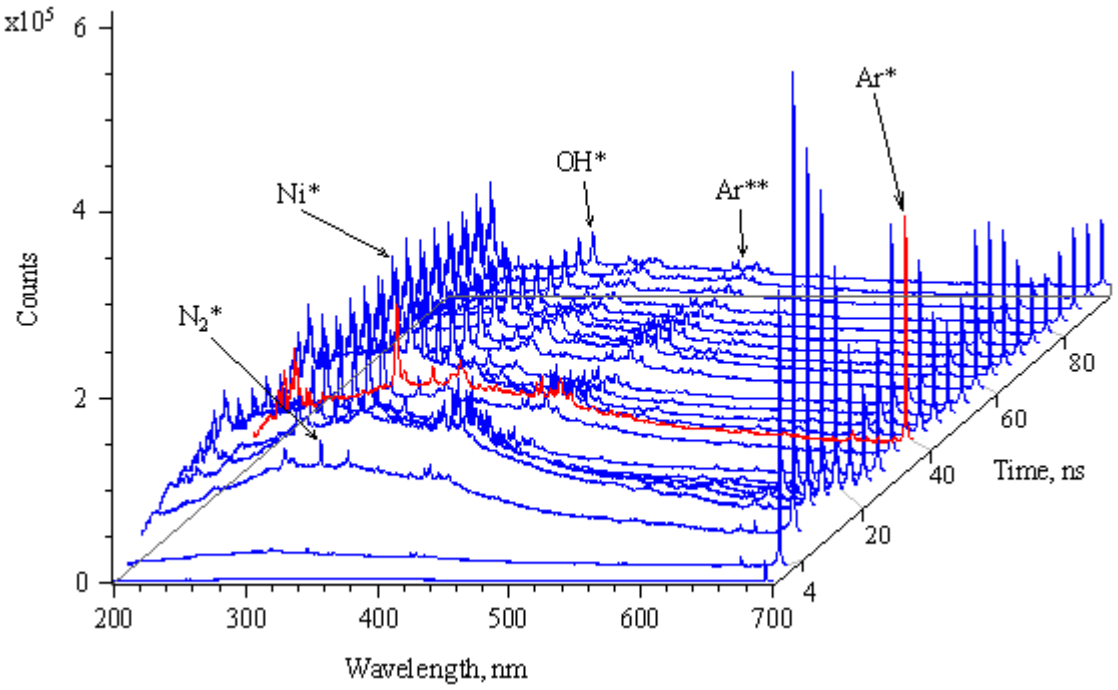

Fig 14. Time evolution of UV-VIS continuum emission in argon discharge at 4 bar

Ar^* (696.5 nm) line, that corresponds to 4p` $\rightarrow$ 4s transition, is used as the diagnostic line. This line with low oscillator strength [17] has negligible reabsorption (unlike most

of Ar^* red lines) and shows oscillations of intensity, which reflect ringing of the pumping (recombination) in the discharge.

Ni^* emission lines is the result of cathode (anode) spots explosion, that appear on the first maximum peak of continuum. Emission from traces of gas impurities (OH^* and N_2^* molecular bands) reflects the purity of the gas mixture in real operation conditions.

4.5. The origin of UV-VIS continuum: bremsstrahlung or photorecombination?

For explanation of the origin of continuum model simulations of photorecombination (4) and bremstrahlung continua (6) were carry out. In both simulations the electron energy distribution function is a key parameter. Usually the Maxwellian function is used in theoretical models. Electron-electron collision is the main mechanism for thermalization of electrons. The non-elastic electron collisions with atoms/molecules disturb Maxwellian distribution out of equilibrium. These two competitive processes determine finally the energy distribution function of electrons in the discharge. Using cross sections for these collisions [1] we estimate that the characteristic time of electron-electron collisions at electron density of 10^{16}–10^{17} cm^{-3} and temperature of 1 eV is of the order of some picoseconds, that is about 10–100 times faster than non-elastic collisions. This estimation shows that electrons really have Maxwellian distribution function in our discharge plasmas.

Model of photorecombination emission

Using expressions (2) and (4) a simple model for photorecombination emission in argon is constructed by taken into account free-bound recombination transitions only to 4s, 4s`, 4p, 4p`, 3d and 3d` levels. These transitions give the main contribution to the photorecombination emission in UV-VIS range. The spectral shape of this emission is sensitive to the electron temperature T_e. Recombination transitions to highly excited Ar^{**} states give the main input to emission in the IR and partly in the red spectral range. The spectral shape of this emission is almost independent on the electron temperature [1, 18]. For determination of photorecombination cross section σ_p the following connection with photoionization cross section σ_i is used [19]:

$$\sigma_p = \sigma_i \frac{g_0}{u_i}\left(\frac{h\nu}{m v c}\right) \qquad (14)$$

where g_0, u_i - statistical weight of excited atomic level and statistical sum of the ground state of the ion respectively. For photorecombination continuum simulation it is not necessary to determine u_i, so it was taken as a constant. Photoionization cross section σ_i data from 4s, 4p and 3d levels as a function of photon energy were taken according to [20]. 4s (4s`), 4p(4p`), 3d(3d`) states consist of 2(2), 8(4), 7(4) sub-levels correspondently, each sub-level has its specific statistical weight g_0 [17]. Details of the model calculation are presented in Appendix 1. Model testing shows that photorecombination intensity weakly depends on the electron temperature T_e, but the continuum spectral shape is rather sensitive to T_e.

Model of bremsstrahlung emission

Several works [2, 3, 4] explain the origin of continuum emission in UV-VIS range by free-free transitions of electrons in collisions with neutral atoms - bremsstrahlung continuum. According to the model (see formula (6)) the bremsstrahlung emission is expressed through the electron-atom elastic collision cross section, which has specific function on the electron energy for different atoms (see, for example, data for all rare gases in [21]). Testing of considered model shows strong dependence of bremsstrahlung emission spectrum on the electron temperature but surprisingly weak dependence on the elastic cross section behavior with electron energy for Ar, Kr, Ne and He rare gases. So the elastic scattering cross section can be replaced by a constant value and taken outside of the integral (6). This modeling result is correlated with our experimental data that continuous emissions in Ar, Kr, Ne and He gases have rather similar UV-VIS spectra. This fact, however, is not sufficient for interpretation of these continua as bremstahlung.

Combination of both models

The spectral shape of experimentally measured UV-VIS continuum spectra (see for example Fig. 14) is difficult to simulate by photorecombination or bremsstrahlung model. We suggest using linear combination of both inputs to continuum emission. According to formula (2) and (6) the intensity of photorecombination is proportional to N_eN_i, (only atomic ions N_i give continuous emission!), intensity of bremstrahlung is proportional to N_eN_a. In plasma with equal densities of electrons and atomic ions bremstrahlung prevails over the photorecombination at low ionization degree and high atom density. In our conditions (N_a of the order of 10^{19}–10^{20} cm^{-3}, $N_e \approx 10^{17}$ cm^{-3}) the key question is: “What is a real fraction of atomic ions in comparison with molecular ones?”

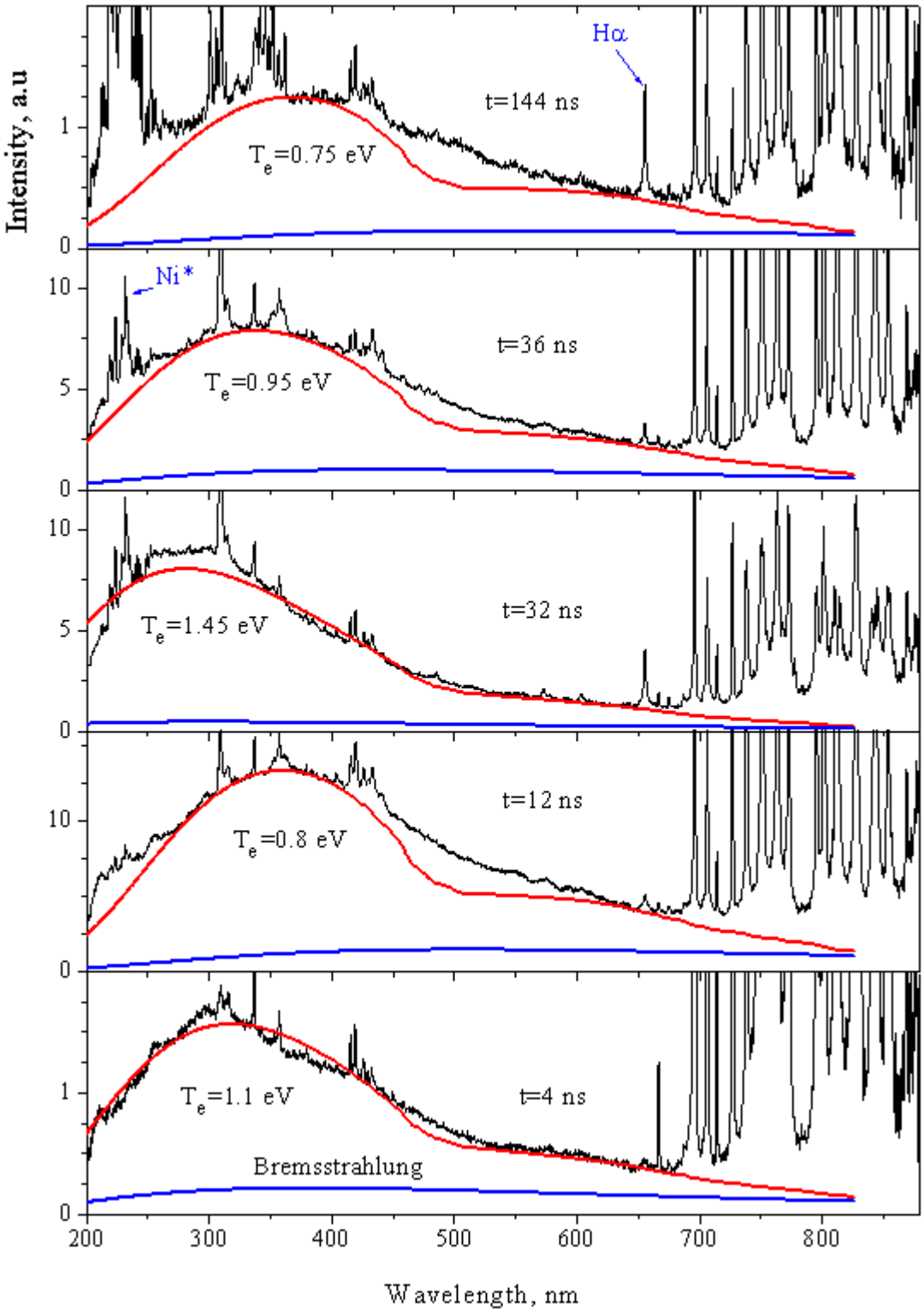

Fig. 15. Time evolution of emission continuum in argon discharge at pressure 4 bar (with 3 mbar additives of H_2). Black curves-experiment (see Fig. 14). Red curves – simulation by combination of photorecombination and bremsstrahlung inputs. Blue curves – input from bremsstrahlung emission.

Dissociative recombination of molecular ions gives only atomic line emission [22] and no continuum emission. It is considered usually that in high-pressure rare gases the fraction of atomic ions is small, because of fast three-body conversion of atomic ions to molecular ions [23] (see reaction (1) in Table 2). However collision of Ar_2^+ ions with fast electrons can destroy them [15] (see reaction (3) in Table 2). Rates of these processes are comparable in our discharge conditions, so the fraction of atomic ions could be rather high.

In spite of the fact that only photorecombination of atomic ions give continuous emission, the rate of this process is very low and main recombination flow is going through the fast dissociative channel. Photorecombination continuum follows the instant density of electrons and atomic ions in the discharge. If most of molecular ions are destroyed to atomic ions, then photorecombination gives the main input to continuum emission. If atomic ions are practically absent, then continuum is caused by bremstrahlung mechanism only. In detail modeling of continuum emission the real ratio between Ar^+ and Ar_2^+ densities is dependent on discharge conditions [15] so inputs of both mechanisms should be taken into account.

Fig. 15 presents time evolution of emission continuum in argon discharge at pressure 4 bar (black curves-experimental data from Fig. 14). Red curves – simulation by linear combination of photorecombination and bremsstrahlung inputs. Blue curves- input from bremsstrahlung emission. Electron temperature T_e and the ratio between these inputs are changed as two free parameters. For rough estimation one can say that the growth of electron temperature, caused by superelastic collisions [23] or oscillations of the discharge voltage, leads to increase of continuous emission in the UV range and decrease in the red side.

4.6. The role of electrons and their temperature to the output of Ar_2^* emission

Energy flow kinetics in high-pressure argon plasma can be considered with a simplified energy-level diagram that is shown in Fig. 16. Table 2 shows main reactions, their rate constants and, as an example, the calculated characteristic reaction times (the following plasma parameters are used: $N_e = 10^{17}$ cm^{-3}, $N_{Ar} = 10^{20}$ cm^{-3} (pressure ~5 bar), T_e = 1 eV).

Table 2. Overview of main reactions and rate constants [14, 15]

	Process	Rate Constant [a)]	Reaction time [b)]
1.	$Ar^+ + 2Ar \rightarrow Ar_2^+ + Ar$	$2.5x10^{-31}$ cm^6 s^{-1}	0.4 ns
2.	$Ar_2^+ + e \rightarrow Ar + Ar^*$	$7.3x10^{-8}$ $T_e^{-0.67} cm^3$ s^{-1}	0.1 ns
3.	$Ar_2^+ + e \rightarrow Ar + Ar^+ + e$	$1.11x10^{-6} e^{-2.94/T_e}$ $cm^3 s^{-1}$	0.2 ns
4.	$Ar^* + 2Ar \rightarrow Ar_2^* + Ar$	$1.0x10^{-32}$ cm^6 s^{-1}	10 ns
5.	$Ar_2^* + e \rightarrow Ar + Ar^* + e$	$1x10^{-8} e^{-1/T_e}$ $cm^3 s^{-1}$	2.7 ns
6.	$Ar_2^*(1_u) + e \leftrightarrow Ar_2^*(O_u^+) + e$	$5x10^{-8}$ cm^3 s^{-1}	0.2 ns
7.	$Ar_2^*(1_u) \rightarrow h\nu + 2Ar$	$3.5x10^5$ s^{-1}	2.9 μs
8.	$Ar_2^*(O_u^+) \rightarrow h\nu + 2Ar$	$2.4x10^8$ s^{-1}	4.2 ns

a) These rate constants are estimated for a gas temperature of T = 350 K.

b) Discharge plasma parameters: $N_e = 10^{17}$ cm^{-3}, $N_{Ar} = 10^{20}$ cm^{-3}, T_e = 1 eV

After a short-pulsed discharge excitation a simplified energy flow scheme looks as follows. Very fast dimerization (reaction 1) of Ar^+ ions to Ar_2^+ ions, dissociative recombination (reaction 2) of Ar_2^+ ions together with electron-collisional and radiative cascades rapidly collapses the excited argon atomic manifold to the lowest excited Ar^* 4s, 4s` states. Ar^* atoms form Ar_2^* molecules in the excited triplet 1_u and singlet O_u^+ states through three-body collisions (reaction 4). Due to their short radiative lifetime only $Ar_2^*(O_u^+)$ species have stimulated emission cross section larger than photo-absorption cross section [14], so only singlet excimer molecules can be used in the lasing effect. The branching ratio for the population of triplet and singlet states in reaction 4 is, according to [14], about 30:1 in favor of the triplet state. Therefore, the yield for the direct production of the lasing state is almost negligibly small. The spin-flip reaction converting triplet into singlet excimers by collision with neutral species have extremely small rate constant [24, 25]. An efficient spin-flip can only be initiated by collisions with free electrons. Complete mixing by electrons leads to the population of triplet 1_u state three times higher than the population of singlet O_u^+ state in according to their statistical weights.

The formation time (reactions 1, 2, 4) of Ar_2^* molecules is about 10 ns after a short excitation pulse. The electron-impact dissociation (reaction 5) of $Ar_2^*(1_u, O_u^+)$ into Ar^* and Ar is about 2.7 ns, that is faster than spontaneous decay of $Ar_2^*(O_u^+)$. So the large fraction of singlet excimer molecules is destroyed by electrons, not by spontaneous emission decay. This harmful process of electron-impact dissociation of excimer molecules is activated, as long as electrons are hot ($T_e \approx 1$ eV) and electron density is high. By decrease of one of these two parameters (N_e or T_e) the absolute quantity of fast electrons decreases and characteristic destruction time increases so the main decay channel for Ar_2^* molecules becomes the spontaneous decay. Electron-impact dissociation of excimer molecules could be the main mechanism responsible for the experimentally observed saturation of Ar_2^* VUV emission output with increase of the pumping power [14, 26].

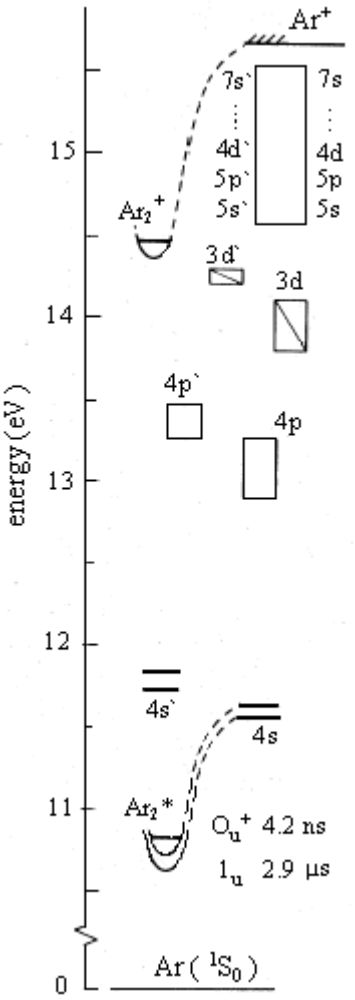

Fig. 16. Simplified energy-level diagram for argon

In the case of Ar_2^+ molecular ion the characteristic time of the "harmful" channel – electron-impact dissociation (reaction 3) is only twice larger than the time of "useful" channel-dissociative recombination (reaction 2). This branching ratio of about 2 is independent on the electron density. If the number of fast electrons is increased in the discharge the "harmful" processes (reaction 3 and 5) prevail over "useful" process (reaction 2) and plasma recombination is delayed.

4.7. Time behavior of electron density and UV-VIS continuum emission in argon plasma

For electron density measurement in high-pressure argon volume discharge small (~3 mbar) hydrogen additives were used. Usually H_β line (486.1 nm) is used as the diagnostic line for determination of electron density [6]. We find that H_β line is very

strongly broadened in our discharge and, as a consequence, its peak intensity is very low. H_α line (656.3 nm) is however easily detectable so this line was used for the diagnostics. Mechanism of H_β, H_α lines excitation in Ar discharge has a separate scientific interest but it is not a subject of this work. Considering the energy diagram for atomic and molecular hydrogen states and experimental kinetics in Fig. 17 the following suggestion is done. Obvious delay of H_α line emission comparing with Ar^* lines at the beginning phase of the discharge is detected. It means that step-wise excitation processes are responsible for H_α line emission. Excitation energies for H_β and H_α lines are 12.75 and 12.09 eV respectively. Zero energy corresponds to the energy of hydrogen atom in the ground state and additionally a binding energy of the hydrogen molecule (4.3 eV) should be taken into account. In the first excitation step electronically excited H_2 molecules could be produced in B $^1\Sigma_u^+$ state (energy ~11.2 eV) by collisions with Ar^* atoms in 4s, 4s` states. The second excitation step is possibly connected with dissociation of H_2^* molecules by energetic electrons (oscillations of H_α line are in phase with electron density oscillations). As a result of this dissociation excited H* atoms are produced.

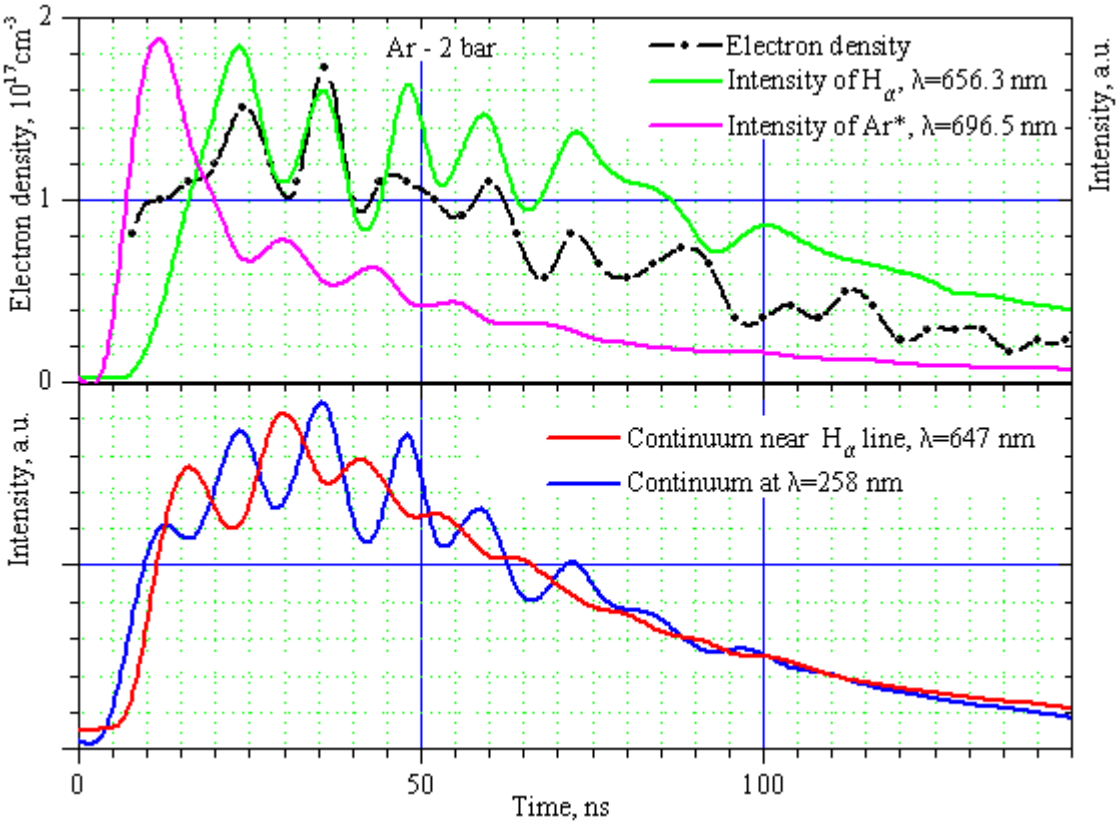

Fig. 17. Time evolutions of H_α line 656.3 nm, red and UV continua and calculated density of electrons for the volume discharge in Ar at pressure 2 bar

Electron density N_e, calculated by formula (8), shows quite a high degree of plasma ionization. Fig. 17 presents time evolutions of H_α line intensity, continua in the red and UV spectral ranges and calculated density of electrons for the volume discharge in argon at pressure 2 bar. H_α line is only weakly excited on the breakdown front and the signal to noise ratio is rather small, that makes difficult exact determination of electron density. The accuracy of these data is about 20 %. Comparing with F_2 –containing gas mixtures, the electron density remains high in argon during rather long time. The same behavior was observed also for the discharge in Kr gas. According to Fig. 17 time behaviors for electron density, intensity of H_α and UV continuum at 258 nm are similar (oscillations are in phase). However, oscillations of red continuum at 647 nm and Ar^* (696.5 nm) line are in the opposite phase with the UV continuum at 258 nm. The reason of different behavior for UV and red continua is caused by change of continuum spectral shape during the discharge (see Fig. 14 and 15).

According to Fig. 18 oscillations of UV continuum at 258 nm and Ar_2^* emission at 126 nm are also in the opposite phase. It means that Ar_2^* emission maxima are temporally overlapped with maxima of red continuum at 647 nm, Ar^* lines and minima of electron density, UV continuum 258 nm and T_e (see Fig. 15).

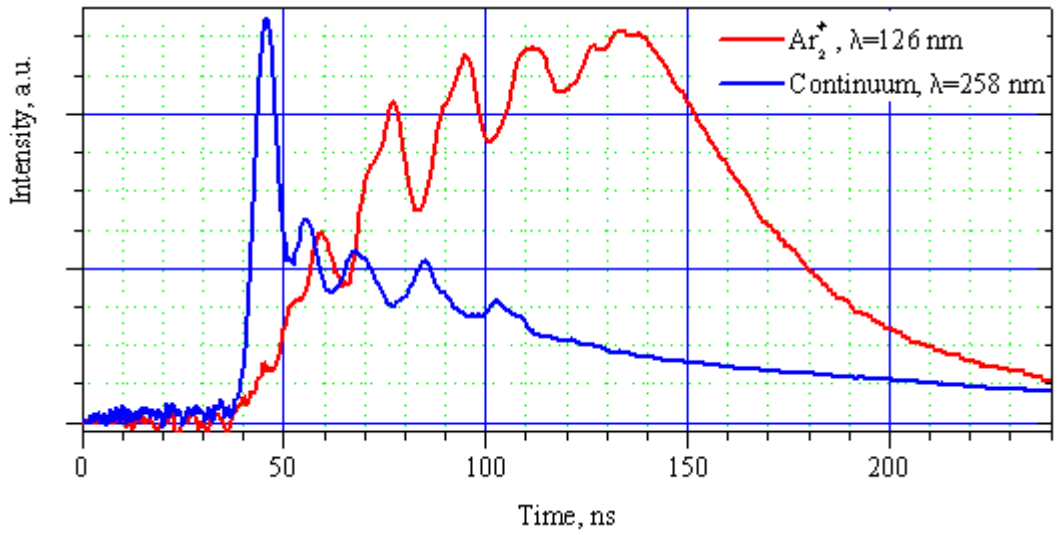

Fig. 18. Kinetics of spontaneous emission of Ar_2* (126 nm) and UV continuum (258 nm) in Ar discharge at 4 bar.

Intensity of Ar^* (696.5 nm) line in the breakdown phase (first 4–8 ns of the discharge in Fig. 17) indicates the population of 4p states by direct excitation of Ar atoms from the

ground state, therefore the first peak of Ar^* is about 4 ns earlier than the first peak of pfotorecombination continuum at 647 nm. In afterglow phase of the discharge 4p Ar^* states are populated mainly by the long oscillated dissociative recombination flow. Each recombination peak (with minimum electron temperature) populates also 4s Ar^* states [27] and give emission peak of Ar_2^* molecules (by reaction 4 in Table 2). It should be taken into account also that rate constants for electron mixing of 4s, 4p Ar^* states are very large [28]. In our conditions characteristic mixing time is about 0.01 ns, therefore Ar^* in 4p and 4s states are in thermodynamic equilibrium.

When the electron temperature and density is maximal (large part of Ar_2^+ ions is destroyed by electron-impact dissociation (reaction 3)), recombination flow and correspondently Ar^* emission comes to minimum which gives minimum also for Ar_2^* emission.

4.8. Some ideas for optimization of discharge pumping

One of the main results of our diagnostics is that fast electrons can destroy excimer Ar_2^* molecules and molecular Ar_2^+ ions, therefore it is useful to cool down electrons as fast as possible after the main pumping pulse. The major electron cooling process in high-pressure gases is the electron energy loss in elastic electron-atom collisions. In one elastic collision with atom the electron loses only a small fraction of its energy. Energy loss differential equation is as follows [1]:

$$\frac{dE}{dt} = -\frac{2m}{M} E \cdot \nu(E) \qquad (15)$$

where M is mass of the atom, $\nu(E)$ is elastic collision rate.

The model calculation of electron energy loss for different rare gases is presented in Fig. 19. Calculations were done for the following conditions: electrons have Maxwellian energy distribution function with initial temperature T_e = 2 eV, pressure of the gas is 6 bar, gas temperature is 350 K, external electric field is absent, non-elastic collisions are not taken into account. Model estimation shows that helium has the maximal rate of electron cooling due to lowest mass between all rare gases. Due to a high mass for Ar and Kr atoms electron temperature in the recombination stage (and as a consequence electron density) falls rather slowly.

Taking into account superelastic collisions ($R^* + e \rightarrow R + e_{fast}$) the cooling of electrons at high pumping conditions will get additional delay. The higher is the density of excited species the longer is delay of the electron cooling. For example, according to [14], after high e-beam pumping (the energy deposition ~15 meV/atom for Ar at 1 bar) the electron temperature remains above 0.7 eV during about 1500 ns.

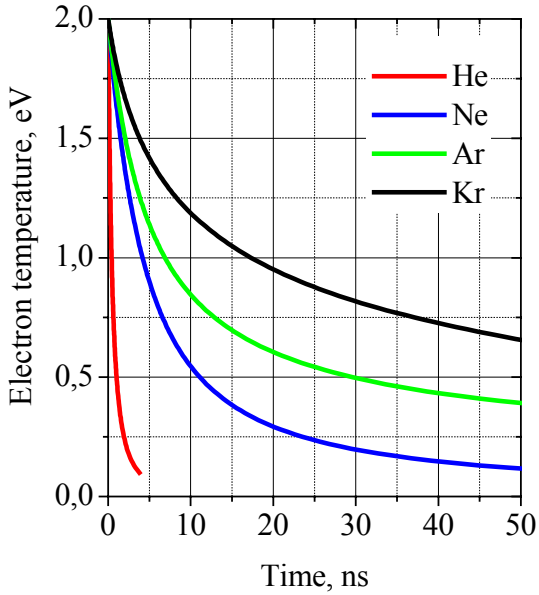

Fig. 19. Electron cooling due to elastic collisions with rare gas atoms

We estimate the energy deposition in our discharge for Ar at 6 bar as about 30 meV/atom, so delay of the electron cooling certainly takes place in our discharge. From one side, high gas pressure helps to accelerate electron cooling by increase of elastic collision rate. From another side, densities of excited species grow with the gas pressure and superelastic collisions delay the electron cooling.

Recommendation for increase of the VUV Ar_2^* emission output

Spontaneous emission of Ar_2^* molecules at 126 nm is the best indicator for optimization of its peak density, which is necessary prerequisite for lasing achievement. For faster recombination electrons should be cooled to the temperature lower than ~1 eV after the main pumping pulse. The cooling could be accelerated with increasing of Ar gas pressure and with additives of helium to the gas mixture. Helium atoms with small mass have the highest efficiency for the electron cooling. The growth of the gas pressure leads to acceleration of three-body Ar_2^* and Ar_2^+ formation reactions (reaction 4 and 1 in Table 2) as a square of pressure. Ar_2^* and Ar_2^+ species can be also effectively formed by reactions

$$\begin{aligned} Ar^* + Ar + He &\rightarrow Ar_2^* + He \\ Ar^+ + Ar + He &\rightarrow Ar_2^+ + He \end{aligned} \qquad (16)$$

One has taken into account, however, that ignition of homogeneous high-current discharge at higher pressure is a serious physical and technical problem.

SUMMARY

In this work high current powerful (~20 MW/cm^3), fast (~10 ns) pulsed volume discharge in high-pressure (up to 10 bar) rare gas mixtures has been investigated with ns time-resolved spectroscopic diagnostic techniques. Importance of this subject is connected with the development of efficient excimer light sources and using rare gas discharge plasma as VUV laser active medium.

Specific aims of this work are: 1. Experimental diagnostics of electron density, determination of its influence to the VUV emission of rare gas excimers, 2. Spectral-time behavior of UV-VIS continuum emission and revealing of its origin.

Stark broadening of helium (501.6 nm) and hydrogen H_α (656.3 nm) line profiles is used for electron density measurement during pumping and afterglow phases of the discharge. Helium and argon mixtures show maximal electron density of about $4 \cdot 10^{16}$ cm^{-3} and $4 \cdot 10^{17}$ cm^{-3} correspondently.

Broad (200–850 nm) UV-VIS continuum is observed for discharge in Ar, Kr rare gases. It was revealed that in pure argon continuum consists of two parts caused by: photorecombination of electron with atomic ions and bremstrahlung of electrons on neutral atoms. The model for continuum simulation is proposed. Continuum spectral shape depends on the electron temperature, which is about 1 eV in Ar discharge. For rough estimation one can say that the growth of electron temperature, caused by superelastic collisions or oscillations of the discharge voltage, leads to increase of continuous emission in the UV range and decrease in the red side.

Possible mechanisms responsible for the experimentally observed saturation of Ar_2^* VUV emission output with increase of the pumping power were analyzed on the basis of received plasma parameters. Fast electrons can destroy excimer Ar_2^* molecules and molecular Ar_2^+ ions, therefore it is necessary to cool down electrons as fast as possible after the main pumping pulse. The cooling could be accelerated with increasing of Ar gas pressure and with additives of helium to the gas mixture.

I wish to thank my supervisor Head of Laboratory of Laser Techiques Alexey Treshchalov for initiating all these investigations, continuous support, help and advices.

REFERENCES

[1] Райзер, Ю. *Основы современной физики газоразрядных процессов*. Москва, «Наука», 1980

[2] Park J., Henins I., Herrmann H. and Selwyn G., *Physics of Plasmas*, **7**, 3141-3144, (2000)

[3] Rutscher A. and Pfau S., On the origin of visible continuum radiation in rare gas glow discharges, *Physica* , **81**, 395 – 402, (1976)

[4] Касьянов, В., Старостин, А., *ЖЭТФ*, **48**, 295-302, (1965)

[5] Иванов, В., Пенкин, Н., *Журнал Прикладной Спектроскопии*, **40**, 5-33, (1984)

[6] Грим, Г. *Уширение спектральных линий в плазме*. Москва «Мир», 1978

[7] Treshchalov, A., Lissovski, A., Chikeyev Y., "High-current discharge pumping of ArF, F_2 lasers without cathode hot spots and filament instabilities," *In: Intern. Conf. on Atomic and Molecular Pulsed Lasers IV, SPIE*, **4747**, 253-260, (2002)

[8] Chikeyev, Y., Lissovski, A., Sonman, A. and.Treshchalov. A., "Spectroscopic diagnostics of pulsed high-current discharge without cathode hot spots", *In: Proc. XVth Europhysics Conference on Atomic and Molecular Physics of Ionized Gases*, Miskolc-Lillafüred, 366-367, (2000)

[9] Treshchalov, A., Lissovski, A., Chikeyev, Y., "Spectroscopic diagnostics of high-current discharges in UV-VUV excimer lasers," *In: Proc. of Intern. Symp. on High Pressure, Low Temperature Plasma Chemistry HAKONE VIII*, Univ. of Tartu, Estonia, 277-281, (2002)

[10] Lissovski, A. and.Treshchalov, A, “Bremsstrahlung emission in high-pressure gas discharges", *In: Proc. XXVIth Intern. Conf. on Phenomena in Ionized Gases*, Greifswald, Germany, **3**, 247-248, (2003)

[11] Boichenko, A., Tarasenko, V. and Yakovlenko, S., *Laser Physics*, **9**, 1004-1020, (1999)

[12] Nighan, W. and Fowler, M., *IEEE Journal of Quantum Electronics*, **25**, 791-802, (1989)

[13] Treshchalov, A., Jalviste, E., Smerechuk, A., Gerasimov, G., Hallin, R. and Arnesen, A., "VUV emission of Kr_2 molecules under high-current sliding discharge excitation" *In: Proc. of Intern. Symp. on High Pressure, Low Temperature Plasma Chemistry HAKONE VIII*, Univ. of Tartu, Estonia, 291-295, (2002)

[14] Neeser, S., Kunz, T. and Langhoff, H., *J. Phys. D: Appl. Phys.*, **30**, 1489-1498, (1997)

[15] Jonkers, J., Sande, M., Sola, A., Gamero, A., Rodero, A. and Muller, J., *Plasma Sources Sci. Technol.,* **12**, 464-474, (2003)

[16] Sauerbrey, R., Emmert, F. and Langhoff, H., *J. Phys. B: At. Mol. Phys.,* **17**, 2057-2074, (1984)

[17] Wiese, W., Smith, M., and Miles, B., *Natl. Stand. Ref. Data Ser. Natl. Bur. Stand.,* **22**, (1969)

[18] Биберман, Л., Норман, Г., *Успехи Физических Наук*, **91**, 193-246, (1967)

[19] Фортов, В., *Энциклопедия низкотемпературной плазмы*, Москва, «Наука», 2000, **1**, 49

[20] Duzy, C. and Hyman, H., *Physical Review A*, **22**, 1878-1883, (1980)

[21] http://www.siglo-kinema.com/database/index.htm

[22] Shiu, Y. and Biondi, M.,*Physical Review A*, **17**, 868-872, (1978)

[23] Elson, E. and Rokni, M., *J. Phys.D: Appl.Phys.*, **29**, 716-725, (1996)

[24] Keto, J., Gleason, R., Bonifield, T. Walters, G. and Soley, F., *Chem. Phys. Lett*., **42**, 125, (1976)

[25] Morikawa, E., Reiniger, R., Gurtler, P. and Laporte, P., *J. Chem. Phys*., **91**, 1462, (1989)

[26] Lam, S., Zheng, C., Lo, Dem'yanov, A. and Napartovich, A., *J. Phys. D: Appl. Phys.,* **33**, 242-251, (2000)

[27] Barrios, A., Sheldon, J. and Hardy, K., *Physical Review Letter*, **69**, 1348-1351, (1992)

[28] Eckstrom, D., Nakano, H., Lorents,D., Rothem, T., Betts, J., Lainhart, M., Triebes, K. and Dakin, D., *J. Appl. Phys*., **64**, 1691-1695, (1988)

KOKKUVÕTE

"Impulsslahenduse spektroskoopiline diagnostika kõrgrõhulistes inertgaasisegudes"

Käesolevas töös on uuritud tugevavoolulist, võimsat (20 MW/cm^3) ja kiiret (~10 ns) impulss-ruumlahendust kõrgrõhulises (kuni 10 bar) inertgaaside segus aeglahutatud spektroskoopilise diagnostika meetodil. Selle temaatika on seotud suure kasuteguriga eksimeer-valgusallikate arendamisega ja inertgaaside lahendusplasma kasutamisega VUV-laseri aktiivkeskkonnana.

Selle töö spetsiifilised eesmärgid on: 1. elektronide tiheduse eksperimentaalne diagnostika ja nende mõju määramine inertgaaside eksimeeride VUV kiirgusele, 2. UV-VIS kontiinuumi spektraalajalise käitumise uurimine ja tema päritolu väljaselgitamine.

Elektronide tiheduse mõõtmiseks pumpamise ja järelhelenduse staadiumides on kasutatud heeliumi joone (501.6 nm) ja vesiniku joone (656.3 nm) profiilide Starki laienemist. Elektrilahenduse korral heeliumi ja argooni segudes on saadud maksimaalseks elektronide tiheduseks vastavalt $4 \cdot 10^{16}$ cm^{-3} ja $4 \cdot 10^{17}$ cm^{-3}.

Lai (200–850 nm) UV-VIS kontiinuum ilmnes uuritud inertgaasides (Ar, Kr). On välja selgitatud, et puhtas argoonis koosneb kontiinuum kahest osast, mis on põhjustatud: elektronide fotorekombinatsioonist atomaarsetel ioonidel ja elektronide pärsskiirgusest neutraalsetel aatomitel. On esitatud mudel kontiinuumi simuleerimiseks. Kontiinuumi spektraalne kuju sõltub elektronide temperatuurist, mis on argooni lahenduses umbes 1 eV. Jämedas lähenduses elektronide temperatuuri kasvuga, mis on tingitud superelastsetest põrgetest või lahenduspinge ostsillatsioonidest, kaasneb kiirguskontiinuumi UV osa suurenemine ja punase osa nõrgenemine.

Saadud plasmaparameetrite alusel on analüüsitud võimalikke mehhanisme, mis põhjustavad eksperimendis vaadeldud Ar_2^* VUV kiirguse küllastumist pumpamise kasvul. Kuna kiired elektronid võivad hävitada Ar_2^* eksimeermolekule ja Ar_2^+ molekulaarioone on vaja jahutada elektrone pärast pumpavat impulssi nii ruttu kui võimalik. Jahutamist võib kiirendada tõstes Ar gaasi rõhku ja lisades gaasisegule heeliumi.

APPENDIX 1.

Mathcad programm

Photorecombination model

1) Photoionization cross sections for Ar from 4s, 4p and 3d states [20]:

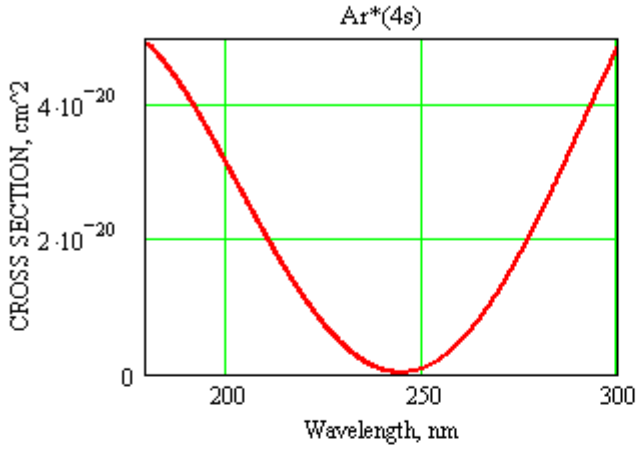

Statistical weights and energies of 4s and 4s' states sub-levels:

$$g_{4s} := \begin{pmatrix} 5 \\ 3 \end{pmatrix} \quad E_{4s} := \begin{pmatrix} 93144 \\ 93751 \end{pmatrix} cm^{-1}$$

$$g_{4s'} := \begin{pmatrix} 1 \\ 3 \end{pmatrix} \quad E_{4s'} := \begin{pmatrix} 94554 \\ 95400 \end{pmatrix} cm^{-1}$$

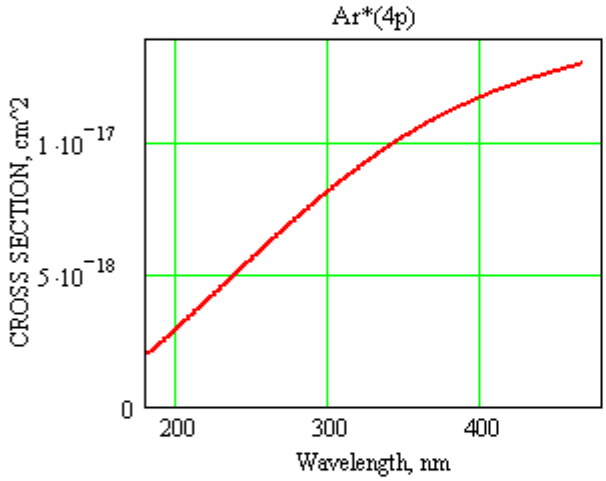

Statistical weights and energies of 4p and 4p' states sub-levels:

$$g_{4p} := \begin{pmatrix} 3 \\ 7 \\ 5 \\ 3 \\ 5 \\ 1 \\ 7 \\ 7 \end{pmatrix} \quad E_{4p} := \begin{pmatrix} 104102 \\ 105463 \\ 105617 \\ 106087 \\ 106238 \\ 107054 \\ 105436 \\ 106436 \end{pmatrix} cm^{-1}$$

$$g_{4p'} := \begin{pmatrix} 3 \\ 5 \\ 3 \\ 1 \end{pmatrix} \quad E_{4p'} := \begin{pmatrix} 107132 \\ 107290 \\ 107496 \\ 108723 \end{pmatrix} cm^{-1}$$

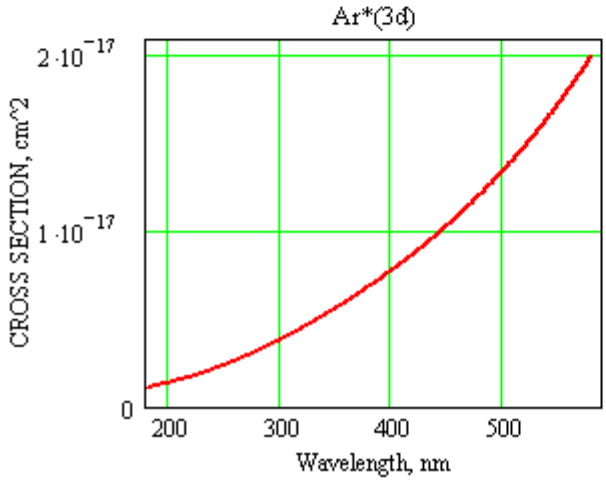

Statistical weights and energies of 3d and 3d' states sub-levels:

$$g_{3d} := \begin{pmatrix} 1 \\ 3 \\ 9 \\ 7 \\ 5 \\ 3 \\ 7 \end{pmatrix} \quad E_{3d} := \begin{pmatrix} 111668 \\ 111818 \\ 112750 \\ 113020 \\ 112139 \\ 114148 \\ 113717 \end{pmatrix} cm^{-1}$$

$$g_{3d'} := \begin{pmatrix} 5 \\ 7 \\ 5 \\ 3 \end{pmatrix} \quad E_{3d'} := \begin{pmatrix} 114641 \\ 114822 \\ 114805 \\ 115367 \end{pmatrix} cm^{-1}$$

2) Example of model

According to expressions (2), (3), (14) the formula for photorecombination emission to specific sublevel is the following

$$J_{sub\_level}(h\nu, kT_e) = C \cdot N_{ion} \cdot N_e \cdot g_{sub\_level} \cdot h\nu^2 \cdot \sigma_{level}(h\nu) \cdot F(h\nu - E_{sub\_level}, kT_e)$$

where, C - constant, N_{ion} - atomic ions density, N_e - electron density,

g_{sub_level} - statictical wieght of sub-level, $\sigma_{level}(h\nu)$ - photoionization cross section

(from 4s, 4p or 3d states),

$F(h\nu - E_{sub\_level}, kT_e)$ - Maxwellian energy distribution function of electrons, T_e - electron

temperature, E_{sub_level} - energy of sub-level

The total photorecombination is the sum of $J_{sub\_level}(h\nu, kT_e)$

$$J_{rec}(h\nu, kT_e) = \sum_i J_{sub\_level}(h\nu)$$

Example:

$N_e := 1 \times 10^{16} cm^{-3}$ $N_{ion} := N_e$

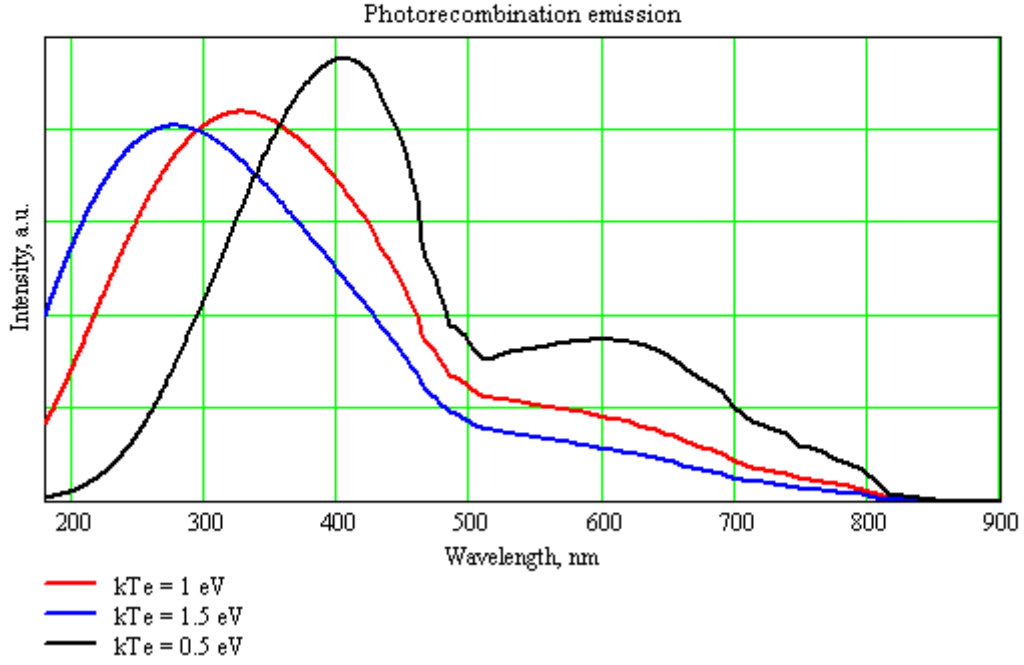

APPENDIX 2.

Mathcad programm

Bremsstrahlung model

Elastic scattering cross sections for Ar [21]

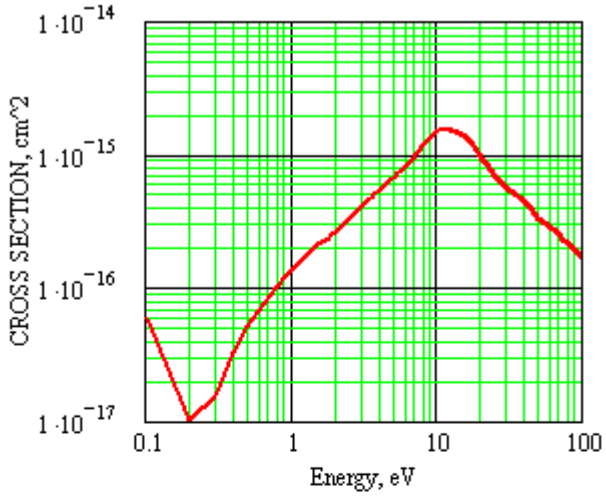

Maxwellian distribution:

$$F(E,kT_e) := const \cdot E^{\frac{1}{2}} \cdot \left(\frac{1}{kT_e}\right)^{\frac{3}{2}} \cdot e^{\left(\frac{-E}{kT_e}\right)}$$

Formulas (5) and (6) are used for simulation of bremsstralung

Bremsstrahlung cross section:

$$Q_B(h\nu,E) := const \cdot \frac{E}{h\nu} \cdot \left(1 - \frac{h\nu}{E}\right)^{\frac{1}{2}} \cdot \left[q_0(E - h\nu) + \left(1 - \frac{h\nu}{E}\right) \cdot q_0(E) \right]$$

Bremsstrahlung emission as a function of foton energy

$$I(h\nu,kT_e) := Const \cdot h\nu \cdot \int_{h\nu}^{100} E^{\frac{1}{2}} \cdot F(E,kT_e) \cdot Q_B(h\nu,E)\, dE$$

Example: Here is presented bremsstrahlung emission as a function of wavelength. Graphics are normalized at $\lambda = 800$ nm. Graphics at kTe = 1 eV and kTe = 0.5 eV are multiplied by factors 3.75 and 64 correspondently.

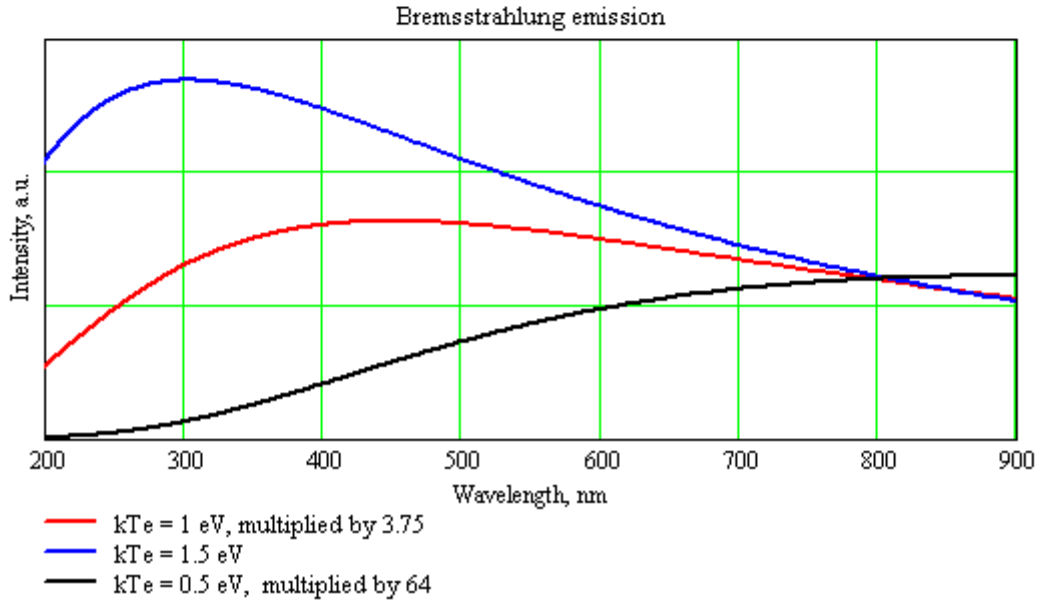

APPENDIX 3.

Mathcad programm

Model of electron energy loss by elastic collisions

Elastic scattering cross sections for He, Ne, Ar, Kr [21]

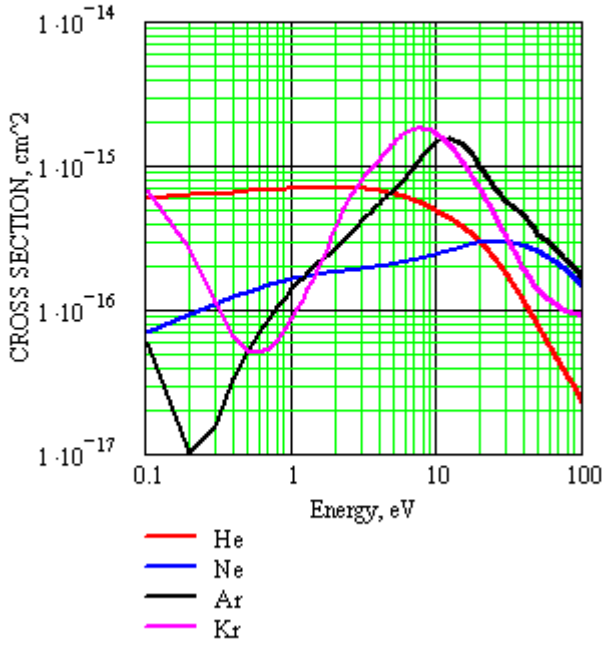

Used formulas:

1. Energy loss differential equation

$$\frac{d}{dt}E = -\frac{2m}{M_a}\cdot E\cdot \nu(E) \qquad (*)$$

2. Elastic collisional rate

$$\nu(E) = N_a\cdot\sqrt{\frac{2E}{m}}\cdot q_0(E)$$

3. Atom mass and density express by

$$M_a = \frac{M}{N_A} \qquad N_a = \frac{p}{k\cdot T_g}$$

M - molar mass, N_A - Avogadro constant, T_g - gas temperature

Solution of equation (*) expresses by T_1 and T_2 - initial and final electron temperature

$$t(kT_1, kT_2) = -\frac{1}{2\sqrt{2m}}\cdot\frac{M}{N_A}\cdot\frac{k\cdot T_g}{p}\cdot\int_{kT_1}^{kT_2} E^{-\frac{3}{2}}\cdot q(E)^{-1}\,dE$$

Example: $p := 6atm$ $T_g := 350K$